

GENERATIVE STATISTICAL 3D RECONSTRUCTION OF UNFOLIAGED TREES FROM TERRESTRIAL IMAGES

Hai Huang, Helmut Mayer

Institute for Applied Computer Science
Bundeswehr University Munich, 85577 Neubiberg, Germany
hai.huang@unibw.de, helmut.mayer@unibw.de, www.unibw.de/ipk/photo

ABSTRACT:

This paper presents a generative statistical approach for the automatic three-dimensional (3D) extraction and reconstruction of unfoliaged deciduous trees from terrestrial wide-baseline image sequences. Unfoliated trees are difficult to reconstruct from images due to partially weak contrast, background clutter, occlusions, and particularly the possibly varying order of branches in images from different viewpoints. This work combines generative modeling by L-systems and a statistical approach for maximum a posteriori (MAP) estimation for the reconstruction of the 3D branching structure of trees. Background estimation is conducted by means of gray scale morphology to provide a good basis of generative modeling. A Gaussian likelihood function based on intensity differences is employed to evaluate the hypotheses. The target tree is classified into three typical branching types after the extraction of the first level of branches and specific Production Rules of an L-system are used. Generic prior distributions for parameters are refined based on already extracted branches in a Bayesian framework and are integrated into the MAP estimation. By these means most of the branching structure besides the tiny twigs can be reconstructed. The results are presented in form of VRML models and show the potential of the approach.

1. INTRODUCTION

Trees are an essential component in city scenes. The detailed 3D representation of individual trees can substantially enhance 3D urban geoinformation by adding natural touch and providing a realistic visualization of city models. Deciduous trees often form the majority of trees in urban areas as they provide shadow in summer while letting the sunlight through in winter. From a practical point of view, for data acquisition for city models terrestrial images are often acquired when trees are unfoliaged, as facades, etc. are more readily visible then. From a scientific, but also a practical point of view, unfoliaged trees have the advantage, that they explicitly show the branches. Yet, to construct 3D models of trees bottom-up/data-driven from wide-baseline image sequences, the branches have to be matched. This is difficult due to the geometric complexity and mutual occlusions of tree branches along with weak contrast and background clutter in the images. Additionally, often the ordering constraint, i.e., a point left of another point on an epipolar line in one image is also left of the corresponding point on the epipolar line in the other image, employed to guide matching, is often not valid for branches even for images taken close to each other.

Former work on tree extraction has focused on aerial images and especially recently laser scanner data. E.g., aerial images are used in (Cheng et al., 2006), which like our work employs a statistical framework consisting also of a generative component. In (Gorte and Pfeifer, 2004) detailed models for trees are extracted from terrestrial laser scanner data.

Like our work, (Sakaguchi and Ohya, 1999) uses terrestrial images. Branches are grown in a volume carved out based on the tree silhouettes in multiple images. (Shlyakhter et al., 2001) generates volumes as in (Sakaguchi and Ohya, 1999) and then 3D medial axes are constructed constrained via an open Lindenmayer-, or in short L-system (Měch and Prusinkiewicz, 1996). In (Reche et al., 2004) volumetric opacity estimation for 3D reconstruction and view-dependent interactive texturing for

visualization are combined. (Neubert et al., 2007) employs 3D particle flow for the estimation of the tree volume in voxel space. (Tan et al., 2007) is based on high quality structure from motion and dense depth estimation and employs shape patterns of visible branches to reconstruct missing parts of trees. The most current approaches are (Chen et al., 2008) and (Tan et al., 2008). Both let the user sketch the trunk and basic branches or the outline of the crown. Trees are then generated by image matching and randomization of existing models from a database. All the given approaches provide plausible results in terms of visualization, but substantial human intervention is needed.

Our work uses the ideas of (Huang and Mayer 2007, Huang 2008) as basis. It presents an approach combining tree modeling by L-systems and statistical sampling, which is able to reconstruct the basic branching structure. We have extended (Huang, 2008) with the following contributions: (1) Background estimation by means of gray scale morphology is employed to remove the relatively thin and mostly dark linear branches as basis for generative modeling. (2) The 3D hypotheses for branches in the form of cylinders are projected into the estimated background and are evaluated with a Gaussian likelihood function based on intensity differences. (3) A Bayesian framework was devised to refine the generic prior distributions for the parameters based on already accepted hypotheses. The improved priors are then integrated into a maximum a posteriori (MAP) estimation. Thus, the results have become more plausible and complete and the sampling more efficient.

The basis of our approach is a highly precise structure from motion procedure (Mayer, 2005) extended to make use of camera calibration information. We manually set the scale for the 3D model. The vertical direction is either derived from the vanishing point of the vertical lines in the images or is defined manually. We assume that trunks correspond to thick, mostly vertical lines. They are verified by matching them in several images using trifocal tensors for prediction. For the remainder

of the paper we assume that the 3D position of the tree is determined by the trunk.

Section 2 describes generative modeling of trees by means of L-systems and background estimation. The generation of 3D hypotheses, the classification of branching types, and the MAP estimation are presented together with the Bayesian refinement of priors in Section 3. Results of experiments on a simulated tree model and trees in real scenes are given in Section 4. The paper ends with conclusions.

2. GENERATIVE MODELING USING L-SYSTEMS

As the bottom-up extraction and matching of branches seems difficult, we model the tree structure as in (Huang, 2008) generatively using L-systems (Měch and Prusinkiewicz, 1996) and extract the tree top-down/model-driven. Particularly, the parameters are determined by statistical sampling to fit the images (cf. Section 3). L-systems are widely used in computer graphics to simulate the structure and growth of vegetation. They represent branching structures in terms of bracketed strings of symbols possibly with associated numerical parameters. The simulation of branching starts with an initial string (axiom). By means of string rewriting substrings of the predecessor string are substituted by successor strings according to a number of Production Rules. Models produced by L-systems show basic botanical features such as a hierarchical structure and self-similarity.

2.1 Branching types

Branching structures of trees can be basically divided into two main groups: “monopodial” and “sympodial” (Deussen and Lintermann, 2005), for which different Production Rules have to be used. The monopodial – m branching system (cf. Fig. 1, m) has a prominent main axis, which is stronger and longer than the side branches. The side branches are again stronger and longer than their side branches of the second order, etc. Because of the dominant axes, monopodial branching structures have a radially symmetric crown.

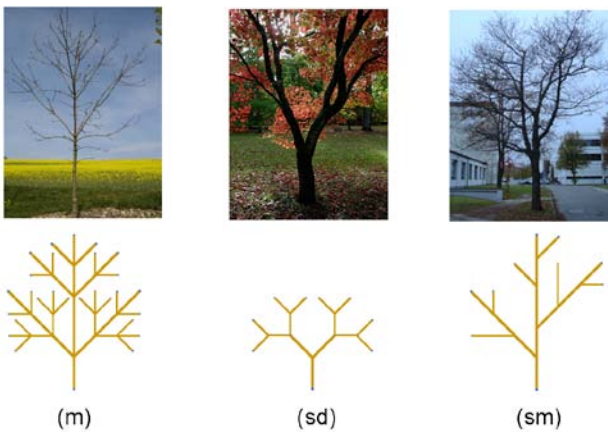


Figure 1: Branching types: (m) monopodial; (sd) sympodial-dichasium; (sm) sympodial-monochasium

Fig. 1 (sd) and (sm) show the two main types of sympodial branching. “Sympodial-dichasium” – sd branching means, that two buds sprout and grow synchronously. Thus, these trees have bilaterally symmetric crowns. The most common branching structure is “sympodial-monochasium” – sm, where

one of the secondary branches has approximately the same direction as the original branch. Sympodial-monochasium branching results into only partially symmetric structures, which still often appear very similar to monopodial branching.

2.2 L-systems

We have devised L-systems for the above branching types with basic Production Rules. As basic entities for the construction of trees we employ cylinders. Compared with (Huang, 2008), the L-systems are extended to dual-variable systems. Additional to the basic Variable “F”, which indicates growth, an additional Variable “I” is employed to control the branching. “I” is only used to derive the next level of string and does not generate any branches.

For example, for monopodial – m trees, the L-system $G_{(m)}$ is defined as follows:

$$G_{(m)} = (V, S, \omega, P)$$

with

- $V_{(m)}$ (Variable): F, I
- $S_{(m)}$ (Constants): +, -, <, >, [,]
- $\omega_{(m)}$ (Initial State): I
- $P1_{(m)}$ (Production Rule): $F = FF$
- $P2_{(m)}$ (Production Rule): $I = F[+>I][-<I]I$,

where the Constants describe rotation around certain axes (“+” and “-” indicate turn left and right – Inclinations; “<” and “>” indicate roll left and right – Azimuths) and the creation of new branches (enclosed by brackets “[” and “]”). The Production Rules instruct to replace “F” and “I” with the given strings in the next iteration.

For instance, starting from $\omega_{(m)} = I$, after two iterations of applying the Production Rules mentioned above (actually two times P2 and one time P1 since there is no “F” in the Initial State), the L-system model becomes:

$$FF[+>F[+>I][-<I]I][-<F[+>I][-<I]I]F[+>I][-<I]I .$$

A graphical example after four iterations (in 2D) is given in Fig. 1 (m).

The Production Rule P1 results after several iterations in branches with a number of connected “F”s. Hence, there are two description levels of branches: the first level is “branch”, i.e., a sequence of “F”s, while the second level is “branch components”, i.e., individual “F”s.

The L-systems for sympodial-dichasium – sd and sympodial-monochasium – sm trees are defined in the same way, but with different Production Rules for “I”:

$$P2_{(sd)}: \quad I = F[+<I][-<I]$$

$$P2_{(sm)}: \quad I = F[+>I]F[-<I]I .$$

A Production Rule can be expressed in parameterized form, e.g.,

$$P2_{(m)}: \quad I = F(l_1, d_1)[+(\beta_1) >(\alpha_1) I][-(\beta_2) <(\alpha_2) I]I ,$$

which indicates the basic parameters:

$$l_i : \text{Length}$$

d_i : Diameter
 α_i : Angle of Azimuth
 β_i : Angle of Inclination .

2.3 Priors

The Production Rules only give a basic description of natural branching. To model real trees, parameters are allowed to vary according to prior distributions.

A generic set of priors is used when the sampling starts and no information about the type of the target tree is available. For the Azimuth α a uniform distribution in $[0^\circ, 360^\circ)$ is used, because most trees have (partially-) radially symmetric crowns. As we employ the full Azimuth, the Inclination β is restricted to the half circle, from -90° (downwards) to 90° (upwards) and we use a normal distribution

$$\beta \sim N(\mu_\beta, \sigma_\beta^2)$$

with mean $\mu_\beta = 45^\circ$ and standard deviation $\sigma_\beta = 20^\circ$ (cf. Fig. 2 red dotted line) reflecting our experience and that for most types of trees the majority of branches points upwards due to phototropism. For length and diameter also normal distributions are used with manually given mean and standard deviation for the first level of branches. For the examples shown in this paper, $\mu_l = 1$ meter, $\sigma_l = 0.3$ meter and $\mu_d = 0.1\mu_l$, $\sigma_d = 0.2d$ were employed. For the higher levels of branches a generic contraction coefficient $\delta = 0.62$, derived from the golden section, was used.

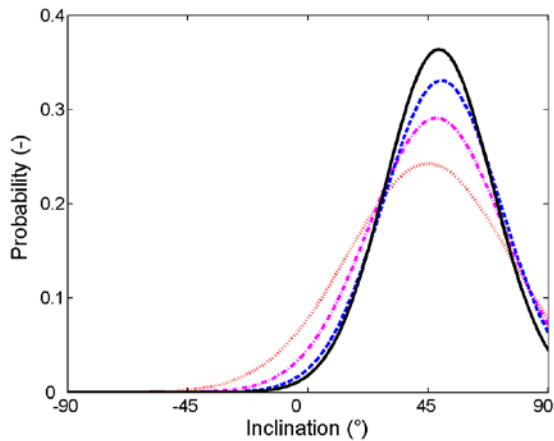


Figure 2: Prior distribution for Inclination and its refinement (example): dotted line (red) – initial prior; dash-dot line (magenta) – after first branch; dashed line (blue) – after second branch; solid line (black) – final prior.

2.4 Background Estimation

For generative modeling, the background clutter has to be modeled. Unfoliated trees mostly consist of relatively thin linear structures and it can be assumed that they have a color different from the background, e.g., sky or building facades. The background is estimated based on gray scale morphological Closing or Opening, the latter for trees brighter than their background, e.g., in night scenes. A circular structuring element, i.e., rotation invariant, is employed to filter linear structures. The size of the structuring element is derived from the projected diameter of the trunk.

Unfortunately, Closing or Opening with such a large structuring element strongly blurs the background. We, therefore, use an iterative recovery process for the background detail. The estimated background is compared with the original image in a sub-domain with a radius of 3 pixels, i.e., smaller than the width of most branches. If the average absolute gray value difference inside the domain is lower than 3 gray values used as an estimate for the image noise, the original value of the current center pixel is inserted into the estimated background. After Gaussian smoothing, the improved background image is used for the next iteration. Fig. 3 shows the original image (left), the result after gray scale Closing (center), and after three recovery iterations (right). For the latter two the histograms below show the gray value differences to the original image. In the histograms the effect of detail recovery, i.e., most small deviations are reconstructed, can be seen more explicitly.

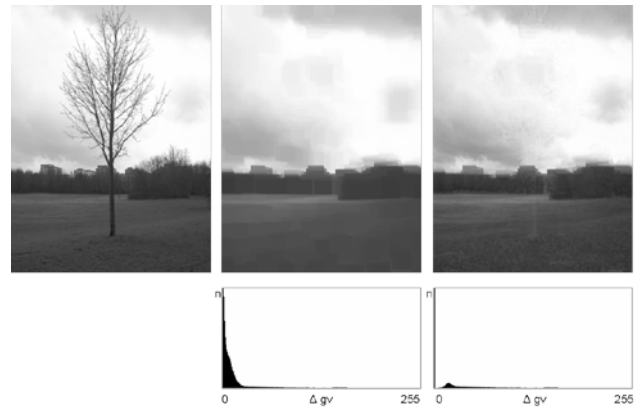


Figure 3: Background estimation: original image (left), after gray scale Closing (center), and after three recovery iterations (right). The bottom row shows the histograms of the gray value differences to the original image.

3. 3D EXTRACTION OF BRANCHES

After locating the trunk by line extraction and matching (cf. Section 1), the branches are extracted. Candidate branches generated by the L-system and parameter sampling are projected into the estimated background images from different viewpoints via the given highly precisely known orientation parameters (cf. Fig. 4). This results in simulated images. Candidates are verified by comparing simulated and original images by means of a Gaussian likelihood function (cf. below).

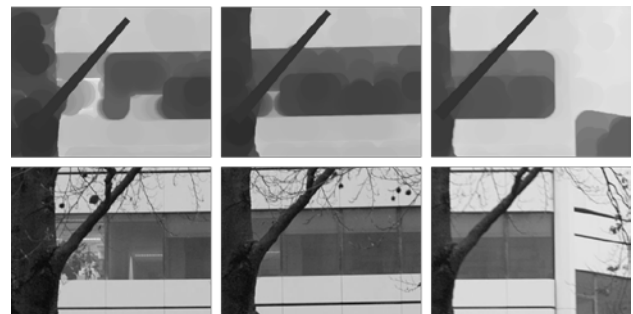


Figure 4: A new hypothesis is projected into the estimated background (top), to be compared with the original images (bottom).

3.1 Classification of Branching Types

After determining the first level of branches, i.e., the branches, which directly grow from the trunk, the branching types are classified. As the branching type is unknown before the extraction and because also the length of the trunk has only been approximately determined, we employ a particularly flexible search for this level by adding the vertical Z-coordinate of the begin point of the branch, i.e., its joint position along the trunk, as an additional parameter (cf. Fig. 5, left). This parameter is sampled together with the branching angles. Thus, branches do not have to start exactly at the given end point of the trunk. The classification is based on the distribution of the joint positions along the trunk.

	Condition 1	Condition 2
monopodial (m)	$\Delta z_{max} \leq \Delta z_{sm}$	$\alpha_{trunk} - \alpha \leq \Delta \alpha_m$
sym.-di. (sd)		$\alpha_{trunk} - \alpha > \Delta \alpha_m$
sym.-mono. (sm)	$\Delta z_{max} > \Delta z_{sm}$	–

Table 1: The two Conditions used for classification of branching types.

As shown in Table 1, we use two Conditions to distinguish the branching types: According to Condition (1) trees are supposed to be of the sympodial-monochasium – sm type if for the maximal difference of the Z-coordinates ΔZ_{max} holds $\Delta Z_{max} > \Delta z_{sm}$, i.e., most of the joint positions of the extracted branches are not concentrated in a relatively small area (cf. also Fig. 5, center); Condition (2) states that if for one of the deviation angles of the branches to the trunk direction holds $\alpha_{trunk} - \alpha \leq \Delta \alpha_m$, i.e., at least one branch follows the direction of the trunk, trees are classified as monopodial – m type (cf. Fig. 5, right), otherwise the branches are assumed to be more suitably described as sympodial-dichasium – sd type.

The appropriate Production Rules of the corresponding L-system (cf. Section 2.1) are then employed for the further levels. As shown below, the priors are refined based on this first level of branches.

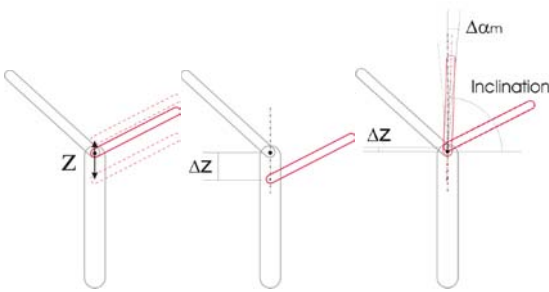


Figure 5: Classification of branching types: additional parameter ΔZ (left), sm type according to Condition1 (center) and m type and sd type according to Condition2 (right)

3.2 Refinement of Priors

During the extraction the distributions of the parameters are refined based on the already extracted branches. This leads to more plausible results and restricts the further search, thus making the sampling more efficient. For context-independent parameters, e.g., Inclinations of branches inside one level, a

Bayesian refinement is used to integrate new evidence. For context-sensitive parameters, i.e., at different branching levels, inheritance and a decay model for the growing space, simulating the influence of the parent and the competition in the neighborhood, respectively, are employed.

We assume that context-independent parameters follow independent and identically-distributed (iid) Gaussians. The initial prior $p(\theta_0)$ is thus refined by new evidence as follows:

$$p(\theta) = p(\theta | \theta_0) p(\theta_0) = N(\theta_i, \sigma_i^2) N(\theta_0, \sigma_0^2) . \quad (1)$$

After multiple evidence has been integrated, the refined prior can be expressed as

$$p(\theta) = \prod_{i=0}^n w_i N(\theta_i, \sigma_i^2) . \quad (2)$$

We give the first evidence the weight $w_1 = 1$. The weight of other evidence is scaled according to the likelihoods $w_i = L_i/L_1 \times w_1$, i.e., $w_i = L_i/L_1$. $w_0 = 2$ is used to give the prior value a slightly stronger weight. After normalization, this means

$$\mu_\theta = \frac{\sigma_\theta^2 \sum_{i=0}^n \frac{w_i \mu_i}{\sigma_i^2}}{\sum_{i=0}^n w_i} ; \sigma_\theta^2 = \frac{\left(\sum_{i=0}^n \frac{w_i}{\sigma_i^2} \right)^{-1}}{\sum_{i=0}^n \frac{1}{w_i}} . \quad (3)$$

An example for the refinement of the Inclination is given in Fig. 2.

For the k^{th} level of branches, with $k > 1$, the context-sensitive Azimuths and Inclinations are assumed to obey Gaussians around the values of their predecessor branches j

$$\alpha_{j,k} \sim N(\alpha_{j,k-1}, \sigma_{\alpha,k}^2) ;$$

$$\beta_{j,k} \sim N(\beta_{j,k-1}, \sigma_{\beta,k}^2) .$$

Initial values are inherited from the parent branches without explicitly considering phototropism or gravity. In the upper levels the density of branches increases, restricting the space for each branch. Assuming that branches grow exponentially

$$N_{k+1} = N_k e^\lambda \quad (4)$$

with N_k the number of branches in the k^{th} level and λ the growth constant, the sequential reduction of the space Φ for an individual branch at level k can be formulated by an exponential decay

$$\Phi_k = \Phi_0 e^{-\lambda k} \quad (5)$$

with Φ_0 indicating the initial space and $-\lambda$ the decay constant. The latter can be derived from the L-system. For a typical sd type tree, $N_1 = N_0 e^\lambda = 2N_0$, and thus λ is $\ln 2$. For sm- and m-trees, λ is $\ln 3$ according to their Production Rules.

As the standard deviations of the angle distributions imply the possible growth space, they also follow the derived exponential decay:

$$\sigma_{\alpha,k} = \sigma_{\alpha,0} e^{-\lambda k}; \sigma_{\beta,k} = \sigma_{\beta,0} e^{-\lambda k}. \quad (6)$$

3.3 Likelihood Function and MAP Estimation

As (Huang, 2008) we use a simple and efficient 2D representation consisting of trapezoids derived from the 3D representation instead of the actual projection of the cylinders. Empirical investigations have shown that the texture of the bark is hard to estimate and shading is not significant for most branches at the employed image resolution.

For the evaluation of the hypotheses we follow (Tu and Zhu, 2006). Assuming that the difference for each pixel follows an iid Gaussian, the likelihood function L can be expressed as:

$$L(D) = \prod_{(x,y) \in D} N(I_s(x,y) - I_o(x,y), \sigma^2), \quad (7)$$

where D indicates the domain of comparison and $I_s(x,y)$ and $I_o(x,y)$ the pixel intensities in the simulated and the original image.

Integrating the refined prior information, the MAP estimation for parameter optimization can be formulated as

$$\hat{\Theta}_{MAP} = \arg_{\Theta} \max \left\{ L(D) \prod_{\theta_i \in \Theta} p(\theta_i) \right\} \quad (8)$$

with Θ the parameter space.

The estimates are computed via a combined Monte Carlo (MC) plus sequential Markov Chain Monte Carlo (MCMC) sampling (Neal, 1993). Since the parameters, especially the branching angles, are distributed sparsely in a relatively large space, plain MC is used in the first coarse sampling phase. The parameters are refined in the second phase. Particularly, the best samples from MC, i.e., ten from one hundred, are taken as candidates for a refined search using ten MCMC iterations for each. The number of candidates is reduced to three after the first round of refinement and the best one is finally found after another twenty MCMC iterations for each of them. Basic MC search is complemented by the Metropolis-Hastings algorithm (Neal, 1993), to avoid local minima.

While in (Huang, 2008) the parameters are sampled in a fixed order, they are now selected based on a probability function

$$g(\bar{\theta}) = g_0(\bar{\theta}) \sum_{\theta_i \in \Theta'} g(\bar{\theta} | \theta_i) g(\theta_i) \quad (9)$$

with

$\bar{\theta}$: current candidate, $\bar{\theta} \in \Theta$;

Θ' : space of parameters sampled in the last step,

$\Theta' \subseteq \Theta$.

This function consists of two parts: (1) the initial probability g_0 , which is derived based on the distributions of individual parameters; (2) a probability conditional to the sampling result

in the last step, which presents the influence of the sampling sequence.

The initial probability is defined in a way giving parameters with a larger search space a higher priority. Table 2 gives an example of g_0 s for the parameters of branches in the first level. For parameters following Gaussian distributions, $g_0 = 2\sigma/\Omega$, where Ω indicates the solution space. For Azimuth and Inclination, the solution spaces are 360° and 180° , respectively. The Ω for length and diameter are approximately limited by 0 and a derived upper limit of $\mu + 3\sigma$. For parameters with uniform distribution $g_0 = 1$.

The parameters sampled in the last step ($\theta_i \in \Theta'$) and their performance influence the current step via a conditional probability:

$$g(\bar{\theta} | \theta_i) = \begin{cases} |\Theta'|^{-1} P_{\text{erf}}, & \forall \theta_i = \bar{\theta} \\ |\Theta'|^{-1}, & \forall \theta_i \neq \bar{\theta} \end{cases} \quad (10)$$

with $|\Theta'|$ the cardinals of Θ' , i.e., the number of parameters that has been sampled in last step, and P_{erf} indicating the performance of the sampling: if the hypothesis was accepted, then $P_{\text{erf}} = 0$, otherwise $P_{\text{erf}} = 1$. To illustrate how this works, a simplified example for the Azimuth is given in Table 3, with $g(\theta_i) = 1$, when $\theta_i \in \Theta'$

Parameter	Distribution	Solution Space (Ω)	g_0
Azimuth	$U[0^\circ, 360^\circ]$	$[0^\circ, 360^\circ]$	1
Inclination	$N(45^\circ, (20^\circ)^2)$	$[-90^\circ, 90^\circ]$	0.22
Length	$N(1, 0.3^2)$	$\approx (0, 1 + 0.9]$	0.32
Diameter	$N(0.1, 0.02^2)$	$\approx (0, 0.1 + 0.06]$	0.25

Table 2: Initial probabilities for parameters in the first level based on their distributions.

Θ'	α	$\alpha+1$	$\alpha+2$	$\alpha+3$	no α
$g(\alpha)_{P_{\text{erf}}=0}$	0	1/2	2/3	3/4	1
$g(\alpha)_{P_{\text{erf}}=1}$	1	1	1	1	1

Table 3: Probabilities for Azimuth α conditional to the selection and the performance in the last step for all possible cases. $\alpha+1$ stands for Azimuth plus one additional parameter, etc. $P_{\text{erf}} = 0$ means the last hypothesis was accepted.

For the sampling of four parameters, the number of all possible combinations is 15. However, assuming that all previously sampled parameters have identical influence on the sampling for the Azimuth in the current step, this number reduces to five: Azimuth alone, Azimuth with 1 to 3 other parameter(s) and any other parameter(s) without Azimuth. Taking the performance of the sampling into account (cf. Equation 10), the probabilities for Azimuth for all possible cases are listed in Table 3.

Generally, (1) if a parameter has not been selected in the last steps, its probability increases; (2) Parameters that led to better results are given a lower priority to keep them basically fixed while other parameters are varied.

4. RESULTS

Current approaches such as (Chen et al., 2008) and (Tan et al., 2008) aim at the efficient generation of realistic looking trees based on significant user input, particularly in terms of the basic tree structure. Opposed to this, we want to demonstrate the potential, but also shortcomings of the devised modeling for trees and their extraction in a fully automatic way with minimal human intervention. For the given examples only the information if the vertical vanishing point is seen horizontally or vertically was given manually.

In our experiments we use images of both simulated tree models and real scenes. The former make it possible to demonstrate the accuracy of the reconstructed results, because 3D ground truth data is available, while for the latter it can be shown how far problems, e.g., with background clutter and weak contrast, can be handled. Because priors are refined, they mostly influence the time needed for a correct result, but not the quality of the result, at least as long as they are not chosen in a totally counter-intuitive way initially.

The input data for our experiments consists of snapshots acquired while simulated models are rotated and wide-baseline image sequences taken unconstrained with hand-held consumer cameras. The output is the reconstructed branching system represented in the form of a VRML (Virtual Reality Modeling Language) model.

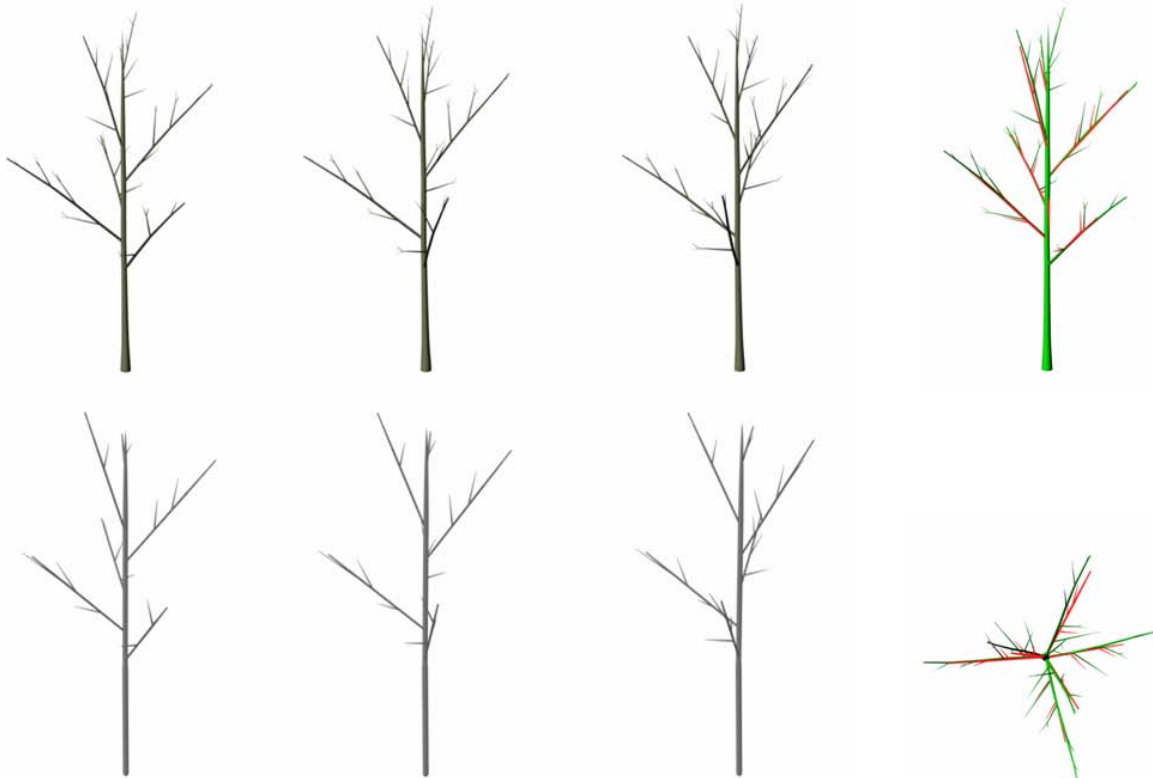


Figure 6: Images of the model of a sympodial-monochasium tree simulated by Xfrog from three of six different viewpoints (top), result from the same viewpoints (bottom), and comparison of simulated (green) and reconstructed (red) model from the front (right top) and the top (right bottom)

5. CONCLUSIONS

We have presented an extended approach for the generative statistical 3D extraction of unfoliated trees from wide-baseline image sequences. After extracting the basic branches

The first experiment uses a simulated model of a sympodial-monochasium tree generated with the software Xfrog. Six snapshots were taken as input images. The result presented in Fig. 6 shows the original (top) and the reconstructed (bottom) model from different viewpoints. Most branches could be reconstructed, even those completely occluded in some views. Fig. 6 (right) shows a comparison from the front and the top. Although the input images cover a relatively small viewing angle (about 45°), the main branches were determined with correct branching angles.

Please note that although an L-system is at the basis of Xfrog, it actually works on an abstraction level with emphases on realistic visualization and ease-of-use. Models produced by Xfrog do not directly follow an L-system, comparable to that used in this work. We, therefore, treat Xfrog models in the same way as real trees without using any extra prior information.

Fig. 7 presents in the top row three of six images showing a young monopodial tree. Below, the reconstruction result is presented from the same viewpoints. While many of the tiny twigs could not be reconstructed, the 3D model consists of most of the branching structure. In Fig. 8 a model of a sympodial-monochasium tree reconstructed from six images is presented. Again, most of the branching structure besides the tiny twigs could be reconstructed.

of the first level, the type of the L-system is determined by means of classification. Hypotheses are projected into an estimated background and are evaluated by an intensity based Gaussian likelihood function. A Bayesian framework is

devised to refine the generic prior distributions for parameters according to already accepted hypotheses. The updated priors are used in the MAP estimation. By these means tree structures can be reconstructed plausibly and efficiently.

Concerning future research, we want to use the improved L-systems presented in this paper to refine individual branches into multiply connected growth components. This makes it possible to model the branches more in detail, e.g., with a curved shape and varying width, by means of generalized cylinders. Reversible Jumps – RJ (Green, 1995) are to be integrated into MCMC for an even more flexible search in conjunction with model selection, e.g., using Akaike's Information Criterion (AIC) (Akaike, 1973), to be able to distinguish between thin twigs and the background.

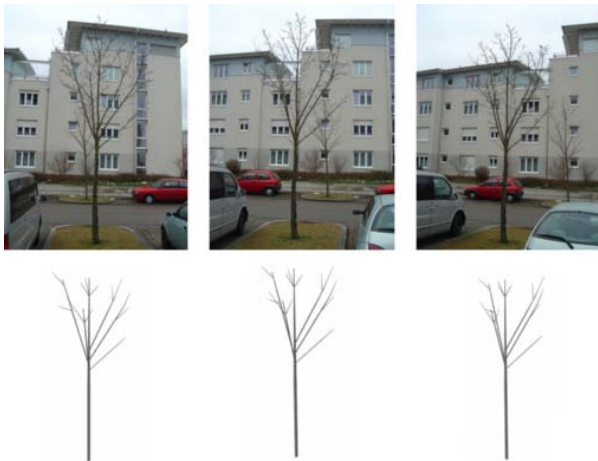


Figure 7: Three of six images of a young monopodial (m-) tree (top) and result from the same viewpoints (bottom).

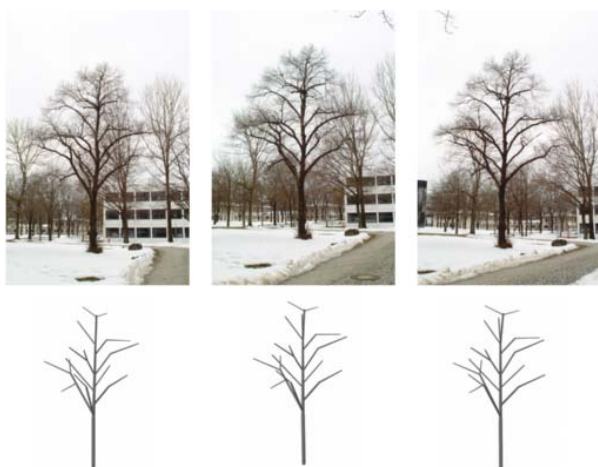


Figure 8: Three of six images of a symodial-monochasium (sm-) tree (top) and result from the same viewpoints (bottom).

Generative statistical modeling is not confined to L-systems. Basically, just a means to construct realistically looking trees that can be efficiently controlled is needed. For this, e.g., (Deussen and Lintermann, 2005) could be a basis. The Production Rules of the L-system could also be refined according to the already found structure. We finally assume

that the upper stages of branches with very thin twigs might be grown stochastically with the derived Production Rules and the learned priors to match the image density.

ACKNOWLEDGEMENTS

We thank Deutsche Forschungsgemeinschaft for supporting Hai Huang under grant MA 1651/12-1 and the anonymous reviewers for their helpful comments.

REFERENCES

- Akaike, H., 1973. Information Theory and an Extension of the Maximum Likelihood Principle. In: *Second International Symposium on Information Theory*, pp. 267–281.
- Chen, X., Neubert, B., Xu, Y. Q., Deussen, O. and Kang, S. B., 2008. Sketch-Based Tree Modeling Using Markov Random Field. *ACM Transaction on Graphics (Proceedings of SIGGRAPH Asia)* 27(5), pp. 1–9.
- Cheng, L., Caelli, T., and Sanchez-Azofeifa, A., 2006. component optimization for image understanding: A Bayesian approach. *IEEE Transactions on Pattern Analysis and Machine Intelligence*, 28 (5), pp. 684-693.
- Deussen, O. and Lintermann, B., 2005. *Digital Design of Nature*. Springer, Berlin, Germany
- Gorte, B. and Pfeifer, N., 2004. Structuring laser-scanned trees using 3D mathematical morphology. *The International Archives of the Photogrammetry, Remote Sensing and Spatial Information Sciences*, 35 (B5), pp. 929-933.
- Green, P., 1995. Reversible jump Markov Chain Monte Carlo computation and Bayesian model determination. *Biometrika* 82, pp. 711-732.
- Huang, H. and Mayer, H., 2007. Extraction of the 3D Branching Structure of Unfoliated Deciduous Trees from Image Sequences. *Photogrammetrie – Fernerkundung – Geoinformation* 2007 (6), pp. 429-436.
- Huang, H., 2008. Terrestrial Image Based 3d Extraction of Urban Unfoliated Trees of Different Branching Types. *The International Archives of the Photogrammetry, Remote Sensing and Spatial Information Sciences* 37 (B3a), pp. 253–258.
- Mayer, H., 2005. Robust Least-Squares Adjustment Based Orientation and Auto-Calibration of Wide-Baseline Image Sequences. In: *ISPRS Workshop in conjunction with ICCV 2005 "Towards Benchmarking Automated Calibration, Orientation and Surface Reconstruction from Images" (BenCos)*, Beijing, China, pp. 1–6.
- Měch, R. and Prusinkiewicz, P., 1996. Visual models of plants interacting with their environment. *SIGGRAPH '96*, pp. 397-410.
- Neal, R.M., 1993. Probabilistic inference using Markov Chain Monte Carlo methods. *Technical Report CRG-TR-93-1, Department of Computer Science, University of Toronto, Canada*.

- Neubert, B., Franken, T. and Deussen, O., 2007. Approximate Image-Based Tree-Modeling Using Particle Flows. In: *SIGGRAPH '07*.
- Reche, A., Martin, I. and Drettakis, G., 2004. Volumetric Reconstruction and Interactive Rendering of Tree from Photographs. In: *ACM Transactions on Graphics*, Vol. 23 (3), pp. 720–727.
- Sakaguchi, T. and Ohya, J., 1999. Modeling and animation of botanical trees for interactive environments. *Symposium on Virtual Reality Software and Technology*, pp. 139-146.
- Shlyakhter, I., Rozenoer, M., Dorsey, J. and Teller, S., 2001. Reconstructing 3D tree models from instrumented photographs. *IEEE Computer Graphics and Applications* 21(3), pp. 53-61.
- Tan, P., Fang, T., Xiao, J., Zhao, P. and Quan, L., 2008. Single Image Tree Modeling. In: *SIGGRAPH Asia '08: ACM SIGGRAPH Asia 2008 papers*, ACM, New York, NY, USA, pp. 1–7.
- Tan, P., Zeng, G., Wang, J., Kang, S. and Quan, L., 2007. Image-based tree modeling. *ACM Transaction on Graphics*, Vol. 26, No. 3, Article 87.
- Tu, Z. and Zhu, S., 2006. Parsing Images into Regions, Curves, and Curve Groups. *International Journal of Computer Vision* 69 (2), pp. 223–249.